

¹ Chapter 1

² Experimental results

³ This chapter contains the measurement results of data taken with diamond sensors.
⁴ The description of measurement setup (section 1.1) is followed by applying experi-
⁵ mental techniques and a discussion of results in order to find operational limitations
⁶ in sections 1.2.1, 1.4 and 1.5. The aim of the chapter is to compare the experimentally
⁷ acquired data with the theory from the previous chapter and to define limitations of
⁸ the diamond detectors in terms of noise, radiation and temperature.

⁹ Diamond sensors are mainly used for two types of measurements: particle counting
¹⁰ and spectroscopy. The first type of measurements depends on the sensor's efficiency
¹¹ – the ability to detect all or at least a known percentage of particles/photons that hit
¹² it. The energy of the radiation is not so important; what bears the information is the
¹³ rate and the spatial distribution. Here the radiation does not necessarily stop in the
¹⁴ bulk, but rather continues its way. In spectroscopy, on the other hand, the idea is that
¹⁵ a particle stops within the sensor, depositing all its energy, which is then measured
¹⁶ via the freed charge carriers. The aim of the experiments described in this chapter is
¹⁷ to 1) quantify the efficiency of the sCVD diamond in counting mode, 2) quantify the
¹⁸ degradation of efficiency with respect to the received radiation dose, 3) quantify the
¹⁹ macroscopic effects on charge carrier behaviour with respect to the received radiation
²⁰ dose and 4) define limitations for its use in spectroscopy.

²¹ The results discussed here show that there are several limitations for using dia-
²² mond as a measurement device. All of them need to be taken into account for the
²³ measurement device to perform reliably and stably. The first step is to build a setup
²⁴ that is insensitive to environmental interferences and minimises electrical noise in
²⁵ the system. The setup needs to be calibrated before use. Then, the measurement
²⁶ conditions have to be defined, such as the temperature, the type of radiation and its
²⁷ flux. This allows us to estimate the lifetime of the detector and predict the longterm
²⁸ change of the signal. This change can then be accounted for when interpreting the
²⁹ output data.

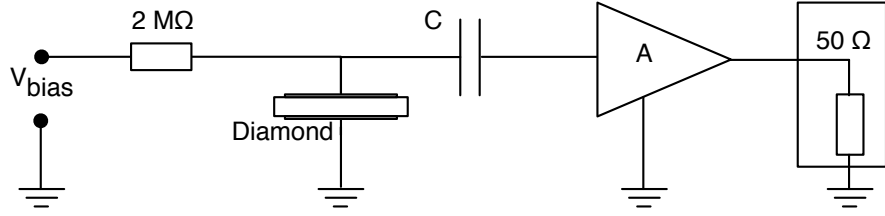


Figure 1.1: Diagram of a diamond detector readout chain.

³⁰ 1.1 Measurement setup

³¹ As said in the introduction, in order to get reliable measurement results, great care
³² has to go towards designing a measurement setup that minimises the noise in the
³³ measurements. In practice this often means using extensive amounts of aluminium
³⁴ foil and cardboard boxes. The foil is wrapped around the exposed parts of the system
³⁵ to shield it from external radio-frequency (RF) interferences. The boxes are usually
³⁶ just put on top of the setup to prevent the light from shining directly onto the
³⁷ sensors. There are of course more professional ways of doing it, but these two items
³⁸ are nevertheless always found in PhD students' labs.

³⁹ The measurements using diamond and explained in these chapters were carried out
⁴⁰ using several setups, but there is a recurring theme to all of them. The measurement
⁴¹ chain consists of three main parts: a diamond sensor, a signal preamplifier and a
⁴² readout device, as seen in diagram 1.1. The signals propagating along the analogue
⁴³ chain (before being digitised by the readout device) are fast – in the GHz bandwidth
⁴⁴ range – and with low amplitudes, which gives rise to importance of RF shielding.
⁴⁵ Also, the connection between the carrier and the preamplifier has to be as short as
⁴⁶ possible to avoid capacitive signal losses in the transmission line. Finally, the system
⁴⁷ needs to be grounded properly.

⁴⁸ 1.1.1 Preamplifiers

⁴⁹ Two preamplifiers were used for the measurements, one sensitive to charge and the
⁵⁰ other to current. *CIVIDEC Cx* (figure 1.2a) is a charge shaping amplifier. Its high
⁵¹ SNR (low noise of 400 electrons and a reported gain of ~ 8.2 mV/fC) makes it a
⁵² good choice for spectroscopic measurements with diamond sensors. *CIVIDEC C2*
⁵³ (figure 1.2b) is a fast current preamplifier with a 2 GHz bandwidth limit. It is
⁵⁴ used for TCT measurements because of its fast response and a good SNR. Both are
⁵⁵ embedded in an RF-tight aluminium box to reduce the noise pickup. Both have an
⁵⁶ AC coupled input and a 50Ω output.

⁵⁷ Calibration

⁵⁸ The amplifiers were calibrated before use to determine their gain. Both were cal-
⁵⁹ ibrated using a square signal generator with a known amplitude step of $U_{in} =$

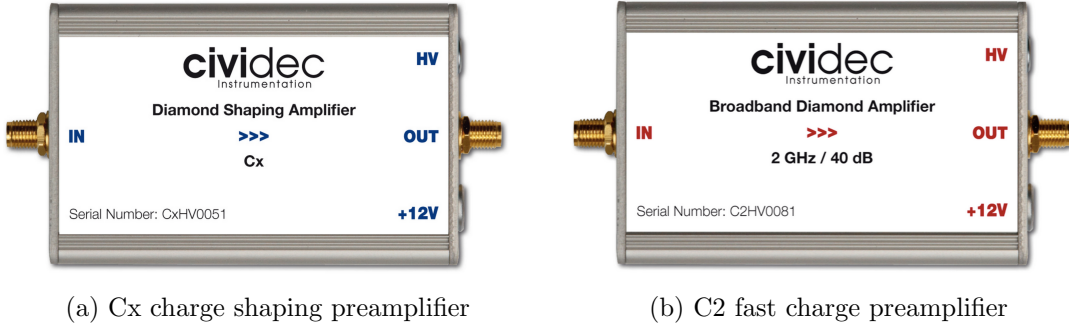


Figure 1.2: Amplifiers used for the charge and current measurements

60 (252 ± 5) mV. A 2 GHz oscilloscope with a 10 GS/s sampling was used to carry
61 out these measurements.

62 In the case of the Cx charge sensitive amplifier, the signal was routed through a
63 capacitor with a calibration capacitance $C_{cal} = (0.717 \pm 0.014)$ pF and then to the
64 input of the amplifier. The pulse area behind the capacitor was $a_{cal} = 5.0 \pm 0.5$ pVs
65 and the signal amplitude on the output was $U_{amp} = (1.95 \pm 0.05)$ V. The input
66 voltage step combined with the calibration capacitance yields a calibration charge
67 $Q_{cal} = C_{cal} \cdot U_{in} = (181 \pm 5)$ fC. The gain of the Cx amplifier is therefore $A_{Cx}^Q =$
68 $\frac{U_{Cx} Q_{cal}}{U_{Cx} Q_{cal}} (9.3 \pm 0.4)$ mV/fC or $A_{Cx}^a = \frac{U_{Cx}}{a_{cal}} = (390 \pm 40)$ mV/pVs. The area-based
69 amplification factor has a higher uncertainty (~ 10 %) than the amplitude-based
70 factor (~ 4 %) due to the measurement limitations of the oscilloscope. Nevertheless,
71 it can be used as an estimate for the integrated charge of a current pulse.

72 To calibrate the C2 current amplifier, only the amplitude gain had to be measured.
73 The input signal amplitude had to be such that it kept the output amplitude within
74 the amplifier's linear range, that is ±1 V. The signal from the generator was therefore
75 routed through a 36 dB attenuator to decrease its amplitude to $U_{inAtt} = (3.95 \pm$
76 0.05) mV. Two amplifiers with different gains were measured, because both were
77 used for the measurements at different times. The output of the first amplifier was
78 $U_{C2-1} = (860 \pm 5)$ mV. This yields the amplification gain equal to $A_{C2-1} = \frac{U_{inAtt}}{U_{C2-1}} =$
79 (217 ± 3) . The second amplifier had the output equal to $U_{C2-2} = (632 \pm 5)$ mV with
80 the gain equal to $A_{C2-2} = (152 \pm 3)$.

81 1.1.2 Diamond samples

82 The diamond detector business is a niche market, with only a handful of producers
83 existing worldwide. Detector-grade diamonds are very difficult to produce, mostly
84 because it is very difficult to ensure a high enough purity of the lattice. It takes
85 companies years of trials to produce high enough quality product. Since the target
86 market are almost exclusively particle physics research institutes, the companies work
87 closely with them to make sure the product is up to par with the requirements. All
88 sensor samples used to carry out these studies were bought at Element Six (E6).

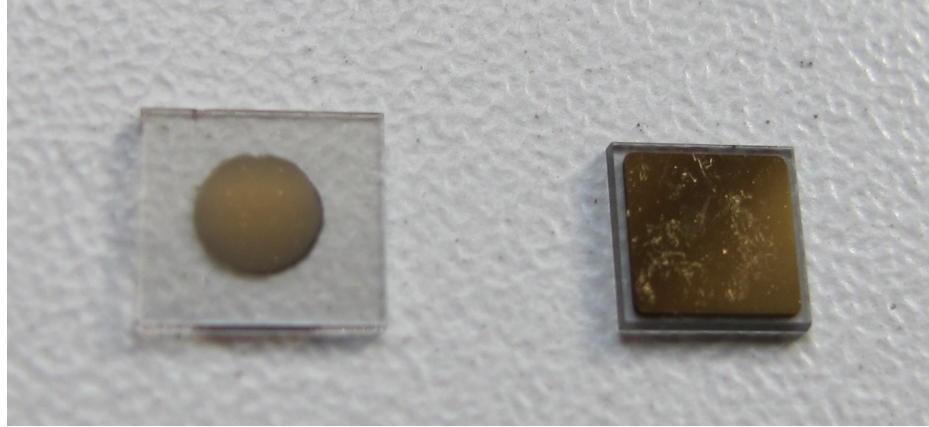


Figure 1.3: Two scCVD diamond samples: A IIa 1scdhq (left) and an E6 S37 (right)

89 They all have the same dimensions, which have become a kind of standard. sCVD
 90 diamonds with dimensions $4.7 \times 4.7 \text{ mm}^2$ are already sufficiently large for most of
 91 the beam monitoring applications and still affordable; the price for sCVD diamonds
 92 grows exponentially with the area. There is also an ongoing race among the producers
 93 to produce larger and larger diamonds while maintaining the price tag. For instance,
 94 a rather young player in this field, IIa from Singapore, has produced high-quality
 95 samples with larger dimensions and the diamond detector community is currently
 96 involved in extensive tests of their products. One of the samples with dimensions of
 97 $5.6 \times 5.3 \text{ mm}^2$ was also sent to the PH-ADE-ID group at CERN to be characterised.
 98 The target thickness for all the samples is $500 \mu\text{m}$. Diamonds this thick yield a high
 99 enough signal-to-noise ratio for MIPs to be measured by the electronics. Table 1.1
 100 shows all the samples used for this study. Two of them were later irradiated with
 101 300 MeV pions and then compared to the pre-irradiated state. Irradiation doses for
 102 damaging the material need to be high – above 10^{12} particles per cm^2 to be able to
 103 observe change in the sensor’s behaviour.

Name	Type	Producer	Dimensions (x, y) [mm ²]	Thickness [μm]	Irradiated
S37	sCVD	E6	4.7×4.7	548	no
S50	sCVD	E6	4.7×4.7	537	no
S52	sCVD	E6	4.7×4.7	515	$1 \times 10^{14} \text{ p/cm}^{-2}$
S79	sCVD	E6	4.7×4.7	529	$3.63 \times 10^{14} \text{ p/cm}^{-2}$
ELSC	sCVD	E6	4.7×4.7	491	no
1scdhq	sCVD	IIa	5.6×5.3	460	no

105 Table 1.1: Diamond sensor samples used

106 The diamond samples have quoted impurity densities of $\leq 2 \times 10^{14} \text{ cm}^{-3}$ and
 107 nitrogen incorporation of $\leq 1 \text{ ppb}$. The electrodes were added by various companies
 108 and institutes. For instance, S52 was metallised by DDL while the Physics Depart-
 109 ment of the University of Firenze, Italy metallised the S79. There are also several
 110 techniques for producing the electrodes. The DDL contacts consist of three layers:
 111 DLC (diamond-like carbon)/Pt/Au with 4/10/200 nm thicknesses, respectively. The

metallisation for S79, on the other hand is made up of Cr/Au with a total thickness of ~ 400 nm. The area coverage also differs from sample to sample. Diamonds must not be metallised until the very edge as the proximity of contacts with a high potential can lead to sparking. However, since only the areas not covered by the metallisation are sensitive, this effectively reduces the sensitive area of the sensors. In the diamonds used here the effective area was anywhere from 9 mm^2 to 18 mm^2 . Leakage current through the bulk was below 1 ns, but increased for the irradiated samples. The capacitance was of the order of (2.0 ± 0.3) pF.

1.1.3 Readout devices

Electrical signals in diamond detectors are in the GHz frequency range. To preserve this information, the readout device has to have a high bandwidth limit. For instance, a 250 MHz limit is enough for the spectroscopic measurements with the Cx charge amplifier, but might be insufficient for the current measurements with the C2 amplifier. Two devices were used take data shown in this chapter. The first choice was a 2 GHz LeCroy WaveRunner 204MXi-A. This specific model has a high enough limit for the fast current preamplifier signals. It offers a versatile solution for analogue signal readout – it is fast to set up and reliable. It is very convenient for use in lab tests and for experiments where small amounts of data are taken and where speed is not crucial. However, its slow acquisition speed turned out to be a bottleneck in the test beam experiment. Its initial 100 Hz readout rate decreased to a mere 20 Hz within 20 minutes, because every single trigger was saved as a separate file and the Windows operating system was not capable of handling 10000+ files in a single directory easily. This is why it was exchanged with a DRS4, an analogue readout device developed by PSI, Switzerland. This compact device is capable of recording up to four waveforms at a time at a steady rate of up to 500 Hz. Its 700 MHz bandwidth limitation was sufficient for the signal from the charge amplifier.

1.1.4 Setup for the efficiency study using β particles

The efficiency study of the diamond sensors was carried out at CERN in a test beam facility called the North Hall. There a straight high-energy particle beam of 120 GeV pions (marked π) was provided to the users to calibrate their detectors. The size of the beam was approximately $\sigma = 10$ mm and the particle rate was of the order of $10^4 \pi \text{ cm}^{-2} \text{ s}^{-1}$. A diamond sensor embedded in a PCB carrier was placed in the beam spot perpendicular to the beam. It was connected via an SMA connector directly to a charge amplifier (described below). The amplified signal was read out using a LeCroy oscilloscope and a DRS4 analogue readout system (both described below). A computer was used as a controller and data storage for the readout device. A separate system was used as a reference detector. The so-called *beam telescope* is a device used to cross-check the measurements of the devices under test (DUTs) and to carry out spatially resolved studies on the DUTs. It consists of several pixellated sensor planes placed in series, which can track a particle's trajectory with a precision

of a few microns. The sensor planes are positioned in front of the DUT and behind it. Then the beam telescope acts as a trigger system – it triggers the readout of both the telescope data and DUT data when both the planes in front and behind the DUT recorded a hit by the impinging particle. A particle detected by all the planes within the DUT window and the DUT itself counts towards its efficiency whereas a hit missed by the DUT counts against it. To discard the hits missing the DUT, a region of interest (ROI) can be chosen in the beam telescope planes.

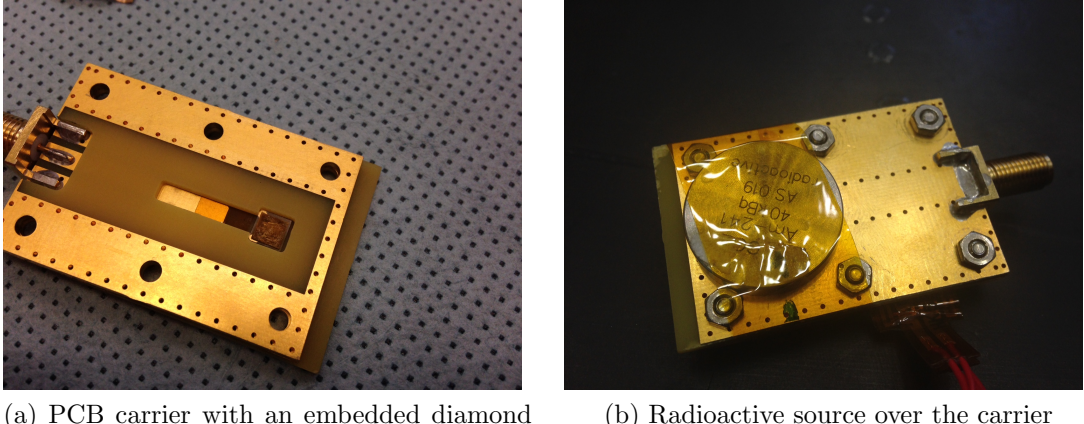
1.1.5 α -TCT setup

Room-temperature TCT measurements were carried out in the lab. The setup consisted of a diamond sensor embedded in a PCB carrier, a current amplifier and an oscilloscope. To measure α particles, their energy loss during their trajectory had to be minimised. Therefore the diamond was placed inside a vacuum chamber. The chamber was a steel tube with a diameter of 5 cm. On one side it was connected to a vacuum pump via an steel pipe. A feedthrough with an SMA connector was placed on the other side. A C2 current amplifier was connected directly onto the feedthrough. The amplified output was connected to the oscilloscope via an SMA cable. An ^{241}Am source with a diameter of 2 cm and a height of 0.5 cm was placed onto the sensor carrier (figure 1.4a) and fixed in place using kapton tape (figure 1.4b). Then the carrier was inserted in the chamber and fixed in place using an air-tight clamp. The pump was then switched on. It was capable of providing the inside pressure as low as 10^{-4} mbar after approximately one hour of operation, but measurements could take place even after five minutes of evacuation, at around 10^{-3} mbar. The most important thing to bear in mind was to switch the bias voltage of the sensor OFF during the process of evacuation, because the air becomes more conductive at the pressure of the order of 10^{-1} mbar. A failure to switch off the bias voltage would cause a spark between the signal and ground line, destroying the amplifier. Yes, this did happen in the course of carrying out these measurements.

1.1.6 Cryogenic α -TCT setup

The experiment at cryogenic temperatures was carried out in the cryolab at CERN. The room-temperature TCT setup had to be modified to allow for measurements at temperatures as low as 2 K. It consisted of three parts: 1) a cryostat – a thermally insulated cylinder capable of containing liquid helium, 2) an inlet – an air-tight mechanical tube with valves and feedthroughs at the top that is lowered in the liquid helium and 3) the diamond sample, a temperature sensor, a heater and cables leading to the feedthroughs.

When the diamond sample was placed in the PCB carrier and the ^{241}Am source was in place, the inlet was sealed and lowered in the empty cryostat. Then the inside volume of the inlet was evacuated to down to 10^{-5} mbar while the liquid helium was flowing into the cryostat. To improve the thermal contact between the diamond



(a) PCB carrier with an embedded diamond sample
 (b) Radioactive source over the carrier

Figure 1.4: Positioning of the α -source on top of the sensor carrier

and the outside of the inlet, a small amount of helium gas was added inside the evacuated inlet, setting the vacuum to around 10^{-3} mbar. This value changed with time, because the gas condensed on the walls of the inlet, reducing the number of floating particles. For this reason the helium gas had to be added from time. This caused a significant undershoot of the sample temperature, which had to be corrected for with the heater. Also, the added gas deteriorated the vacuum inside the inlet. It was very important to monitor the pressure so as not to let it rise above 10^{-2} mbar. The air at this pressure is significantly more conductive and could cause a short circuit between the two diamond plates or in the SMA connectors, destroying the amplifier. Actually, it once did. Furthermore, at approximately 60 K the helium gas had to be evacuated from the inlet to avoid a potential explosion due to the expansion of the gas with temperature. Anyway, when the sample was cooled to the minimum temperature achievable by use of liquid helium without over-pressurising it (4.2 K), the measurements started. After every temperature data point, the current through the heater placed in the PCB next to the diamond sample was increased, warming up the sample. The initial temperature time constant of the order of tenths of seconds at low temperatures increased with temperature and even more so when helium was evacuated from the inlet at 60 K, removing the thermal bridge between the wall of the inlet and the diamond sample. At RT, the time constant was already of the order of minutes.

211 1.2 Particle and photon pulses and spectra

212 In previous chapter the ionisation profiles for different types of radiation were dis-
 213 cussed. It is known that β particles and γ radiation both create a triangular pulse
 214 whereas α particles create a rectangular one. However, their amplitude, width and
 215 rise/fall time depend heavily on the type of interaction with the diamond, the purity
 216 of the diamond and the bandwidth of the amplifier and the oscilloscope. This section
 217 shows the signal pulses of α , β and γ radiation with their respective energy distribu-
 218 tions for the case of a diamond detector. Then follows a discussion of effects of noise
 219 on these measurements.

220 A CIVIDEC C2 current amplifier together with the LeCroy oscilloscope (both
 221 with a bandwidth limit of 2 GHz) was used to record the pulse shapes whereas the
 222 Cx charge amplifier was used for area distribution measurement. A 2 GHz bandwidth
 223 limit defines the minimum rising time equal to $t_r \simeq \frac{0.34}{BW} = \frac{0.34}{2 \times 10^9} = 170$ ps, therefore
 224 the system is capable of measuring pulses with a minimum FWHM $\simeq 170$ ps. This
 225 already makes impossible to measure the initial peak in α response due to the two
 226 flavours of charge carriers travelling. If the flavour travelling through the bulk takes
 227 $t_{t1} \sim 6$ ns to get to the electrode on the other side ($d_1 \sim 500$ μm), the other with
 228 a shorter path to the closer electrode – max. $d_2 \sim 10$ μm – already recombines in
 229 $t_{t2} \sim \frac{d_2}{d_1} t_{t1} = 120$ ps. This is too fast for the C2 amplifier or the oscilloscope to be
 230 able to observe.

231 Figure 1.5 shows a set of pulses and an averaged pulse for α , β and γ radiation as
 232 measured by the non-irradiated sCVD diamond S37. α particles always produce the
 233 same signal pulse, with a high noise RMS. The averaging suppresses the noise while
 234 still retaining most the information. It does, however, smear the rising and falling
 235 edge, increasing the rise time. The t_r is now of the order of 0.5 ns. Both β and γ
 236 pulses look similar - triangular and with a wide range of amplitudes. Here the pulse
 237 count is low, so the really high pulses were not recorded, because they are very rare.
 238 A trigger set very high would be needed to "catch" them with the oscilloscope.

239 1.2.1 Noise limitations

240 Noise is a major limiting factor in particle detection. It defines the minimum measur-
 241 able particle energy and the minimum measurement resolution. It is hence important
 242 to minimise the electric noise in the detector signal. The major noise contribution
 243 comes from poor shielding from external electromagnetic sources. These often cause
 244 so-called ringing, whereby the signal oscillates with a frequency defined by the ex-
 245 ternal source. The ringing makes high-frequency measurements impossible. Another
 246 source of noise is the sensor itself. In the case of silicon, natural light increases the
 247 number of thermally excited free charge carriers, increasing the leakage current. This
 248 is not the case for diamond, which is with its high energy band gap insensitive to
 249 visible light. Nevertheless, any noise produced by the sensors is amplified by the
 250 signal amplifiers, which add an additional noise of the analogue electrical circuit to
 251 the amplified signal. Finally, the digitisers add the quantisation noise to the digitised

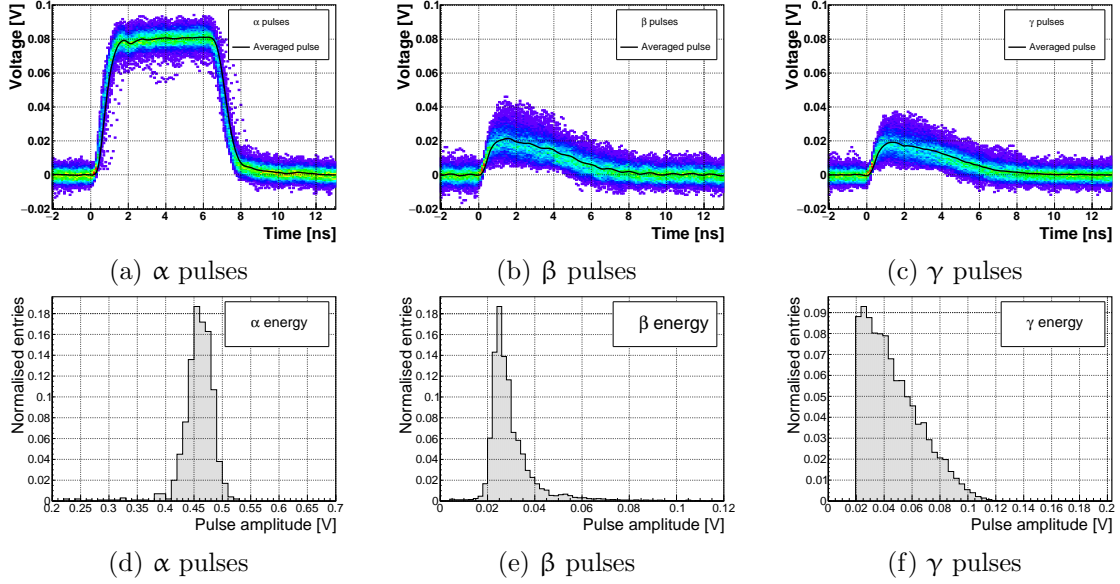


Figure 1.5: Superimposed and averaged pulses (a, b and c, current amplifier) and distributions of deposited energy (d, e, f, charge amplifier) for three types of radiation. Mind the scale on the X axis of the distributions.

252 signal. If the measurement range is significantly higher than the actual measured
 253 signal, the quantisation noise can be a significant contributor to the decrease of the
 254 overall measurement resolution.

255 1.3 Radiation limitations

256 Exposure to ionising radiation degrades sensors. It introduces so-called charge traps
257 by damaging the sensor material. The electrons and holes created by the impinging
258 particle get trapped in these traps, decreasing the induced current on the electrodes.
259 This yields a lower integrated charge in an irradiated sensor than that in a non-
260 irradiated one. Charge collection efficiency is therefore correlated with the level of
261 irradiation. This section tries to study the effects of pion ($\pi_{300\text{ MeV}}$) irradiation on the
262 efficiency of sCVD diamond detectors. To carry out this study, two diamond samples
263 were irradiated to $1 \times 10^{14} \pi \text{ cm}^{-2}$ and S79 to $3.63 \times 10^{14} \pi \text{ cm}^{-2}$. Then a test beam
264 campaign was carried out to observe the charge collection efficiency at different bias
265 voltage settings. The highest achieved efficiency values were used to determine the
266 effective drop in efficiency with respect to received radiation dose. A model defined
267 by a collaboration researching diamond behaviour called RD42 was applied to the
268 measured values and a damage factor was extracted. The factor agreed quite well
269 with the results obtained by the RD42. The next subsection contains measurements
270 and results of a long-term stability study using α and β particles. It is shown that the
271 charge collection efficiency of the irradiated samples improves in time for β radiation,
272 but deteriorates severely for α radiation. To investigate this effect on the scale of
273 charge carriers, the change of TCT pulses with time is observed. Finally, a procedure
274 that improves the pulse shape and with it the charge collection is proposed.

275 1.3.1 Quantifying radiation damage in diamonds

276 The last few decades have seen extensive efforts put into understanding and quan-
277 tifying radiation damage in semiconductors. This varies with the type of radiation
278 (particles or photons) and its energy. There are models existing that try to explain
279 the impact of irradiation and to provide *hardness factors* to compare the radiation
280 damage between different particles. The standard way is to convert the damage into
281 *neutron equivalent*. Some models have been extensively verified with simulations and
282 experimentally. In these experiments charge collection in sensors is measured before
283 and after irradiation. This procedure is repeated several times, with a measurement
284 point taken after every irradiation. When a set of measurements of charge collection
285 is plotted against the radiation dose received by a specific particle at a specific energy,
286 a damage factor k_λ can be extracted. Damage factors have to be measured across a
287 range of energies and types of particles (photons) to properly quantify the damage
288 in the sensors. They are then compared against the simulations to verify that the
289 experimental observations are in line with the theory.

290 Radiation damage in silicon, for instance, is well understood and explained. Sili-
291 con sensor is relatively cheap and widespread, which facilitates the irradiation exper-
292 iments. Diamond, on the other hand, is an expensive material and the technology
293 is relatively new as compared to silicon. Therefore not many institutes are carrying
294 out diamond irradiation studies. To join the efforts, a collaboration called RD42 was
295 formed. It gathers the experimental data from diamond irradiation studies. Unlike

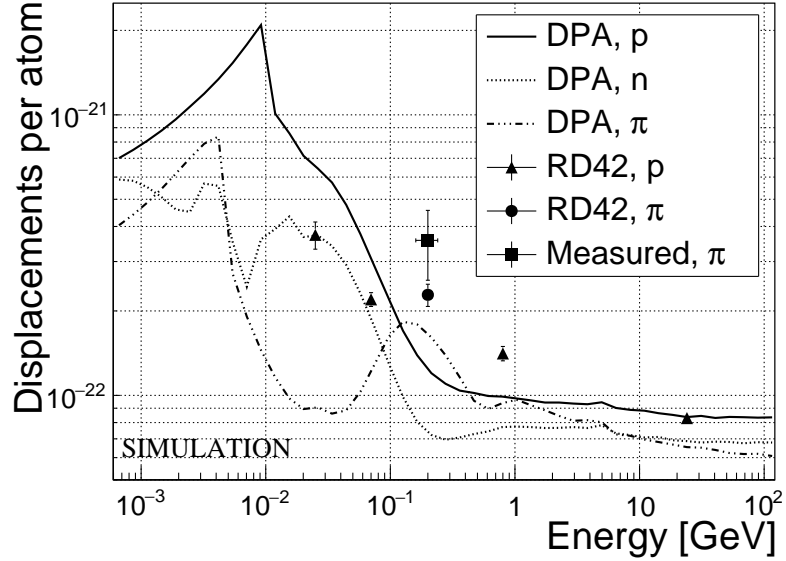


Figure 1.6: Diamond radiation damage - a model based on displacements per atom, courtesy Karlsruhe Institute of Technology [1]. Added are data points for protons and pions by RD42 and one data point for pions measured in the scope of this thesis.

with silicon, the experimental results so far show no significant correlation with the NIEL (non-ionising energy loss) model [2], which correlates detector efficiency with the *number of lattice displacements*. Therefore an alternative model was proposed by Karlsruhe Institute of Technology [3], correlating the diamond efficiency with *displacements per atom* (DPA) in the bulk. Figure 1.6 shows the DPA model for a range of energies of proton, pion and neutron irradiation in diamond. According to the plot, a 300 MeV pion beam damages the diamond bulk twice as much as a 24 GeV proton beam. The data points obtained by RD42 are also added to the plot. They have been normalised to damage by 24 GeV protons. In the end, the data point measured in the scope of this thesis was added for comparison.

306 Pion irradiation

307 Paul Scherrer Institute (PSI) is the largest research institute for material sciences in
 308 Switzerland. Among other tasks they also carry out irradiation campaigns. They
 309 use a beam of 300 MeV/c pions π (kinetic energy 191.31 MeV) with a flux of up to
 310 $1.5 \times 10^{14} \pi \text{ cm}^{-2} \text{ day}^{-1}$. The machine has a 10 % uncertainty on the beam energy.
 311 In addition, due to the uncertainty on the hardness factor, the equivalent fluences
 312 have an error of ± 20 %. Looking at figure 1.6, $\pi_{300 \text{ MeV}}$ sit on a steep section of the
 313 DPA function. After fitting a linear function to this part of the function (marked
 314 red), the error on the DPA due to the uncertainty on the beam energy amounts to
 315 7 %. Overall error on the fluence is therefore the root mean square of the uncertainty
 316 on the DPA and the uncertainty on the hardness factor: $\sigma = 21$ %.

³¹⁷ Two diamond samples, S52 and S79, were exposed to the pion beam in the 2014
³¹⁸ PSI irradiation campaign; S52 to $(1 \pm 0.21) \times 10^{14} \pi \text{ cm}^{-2}$ and S79 to $(3.63 \pm 0.77) \times$
³¹⁹ $10^{14} \pi \text{ cm}^{-2}$. During the process, the golden electrodes got slightly activated, but the
³²⁰ activation decayed in two weeks.

³²¹ Charge collection distance

³²² Three diamonds – non-irradiated S37 and irradiated S52 and S79 – were exposed to a
³²³ 120 GeV test beam before and after irradiation to estimate the charge collection dis-
³²⁴ tance (CCD) and its decrease after irradiation. The samples were primed ("pumped")
³²⁵ prior to data taking using a ⁹⁰Sr radioactive source. Data were then taken at a range
³²⁶ of bias voltages from 30 V to 500 V, yielding up to 1 V/ μm electrical field in the bulk.
³²⁷ Every data point contained approximately 5×10^4 measured particles. The charge
³²⁸ deposited by the particles was measured using a CIVIDEC Cx charge preamplifier.
³²⁹ As expected, the integrated amplitude spectrum followed a landau distribution. Its
³³⁰ most probable value (MPV) was used to calculate the most probable collected charge
³³¹ Q_i :

$$Q_i [e] = Q_i [fC] \cdot 6.241 \times 10^{18} = \frac{MPV [mV]}{A [mV/fC]} \cdot 6.241 \times 10^{18} \quad (1.1)$$

³³² where $A = 9.2 \text{ mV/fC}$ is the preamplifier gain factor. The CCD was then calculated
³³³ using the average number of electron-hole pairs produced per micrometer in diamond
³³⁴ $\delta_d = 36 \text{ e-h } \mu\text{m}^{-1}$:

$$CCD = \frac{Q_i}{\delta_d} \quad (1.2)$$

³³⁵ The resulting CCD for the three measured samples at bias voltages ranging from
³³⁶ $0.2\text{--}1.6 \text{ V } \mu\text{m}^{-1}$ is shown in figure 1.7a. S37 exhibits full collection distance already
³³⁷ at $0.4 \text{ V } \mu\text{m}^{-1}$ whereas the irradiated samples have a more gentle increase of CCD
³³⁸ with increasing bias voltage. It is evident that at $1 \text{ V } \mu\text{m}^{-1}$ the maximum CCD has
³³⁹ not been reached in the case of S79 and S52.

³⁴⁰ Irradiation damage factor

³⁴¹ The irradiation damage factor k is a way to quantify irradiation damage of a specific
³⁴² particle at a specific energy. Via this factor different types of irradiation can be
³⁴³ compared. It is obtained experimentally by measuring the CCD of a number of
³⁴⁴ samples at various irradiation steps and fitting the function 1.4 to the data. λ is the
³⁴⁵ measured CCD, λ_0 is the CCD of a non-irradiated sample and Φ the radiation dose.

$$\frac{1}{\lambda} = \frac{1}{\lambda_0} + k_\lambda \cdot \Phi \quad (1.3)$$

$$\lambda = \frac{\lambda_0}{k_\lambda \lambda_0 \Phi + 1} \quad (1.4)$$

³⁴⁷ The data points with the maximum CCD obtained in the test beam measurements
³⁴⁸ were plotted against radiation dose received (see figure 1.7b). Function 1.4 was fitted

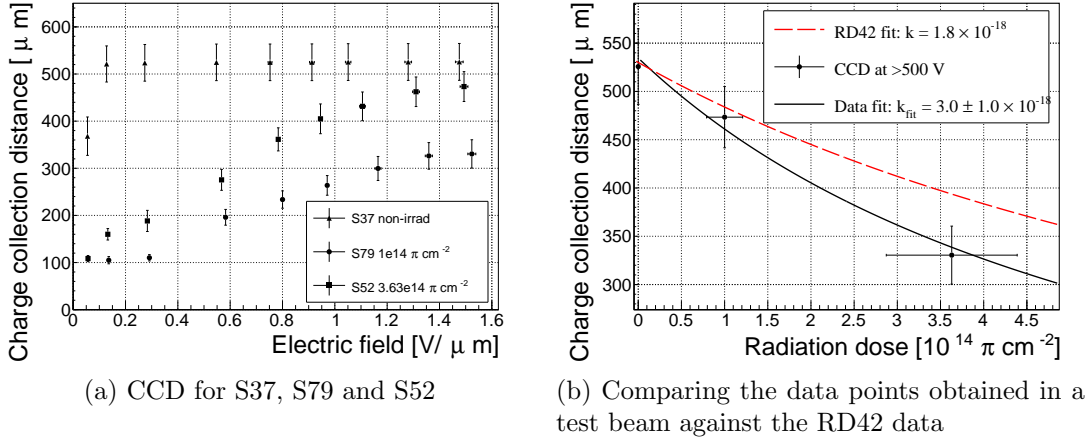


Figure 1.7: The charge collection distance at 500 V bias voltage for the three diamond samples was compared to the RD42 data for pion irradiation. The data points are for about 5–15 % lower than expected from the RD42 data.

to the data points and a damage factor $k_\lambda = (3.0 \pm 1.0) \times 10^{-18} \mu\text{m}^{-1} \text{cm}^{-2}$ was obtained. This value is for a factor of two higher than the damage factor obtained by RD42. A possible cause is that the irradiated samples did not yet have a full charge collection at $1.5 \text{ V } \mu\text{m}^{-1}$. Also, with only two samples measured, the statistical uncertainty was high. Nevertheless, it can be concluded that the 300 MeV pions damage the diamond bulk more than the 24 GeV protons.

1.3.2 Long-term measurement stability

An important requirement for particle detectors is stable performance over long periods of time. For instance, the charge collection for a defined type and quantity of radiation must not change over time or has to change in a predicted way. Diamonds are arguably stable, as long as their environment and operating point does not change. The stability of diamond detectors depends on many external factors. The aim is to study the behaviour of diamond under controlled conditions, with the goal to understand its limitations. One of these limitations is for sure the received radiation dose. It might affect the long-term stability of the sensor during operation.

The three diamond samples (S37, S79 and S52) were exposed to two different types of ionising radiation for a longer period to see if their behaviour changes over time. Two parameters were observed in particular: 1) charge collection of β particles and 2) charge collection and ionisation profile of α particles. The results showed in both cases that *priming* plays an important role in diamond measurement stability. The β particles have a healing effect on the diamond; MIP detection is therefore rather stable in the long run, despite the degradation due to irradiation. Alpha particles, on the other hand, deteriorate the measurement by introducing space charge into the sensor bulk.

373 **β measurements**

374 The samples were intentionally not primed before the measurements took place. The
375 same initial conditions are usually found in HEP experiments. The measurement
376 setup consisted of a diamond sample with the Cx spectroscopic amplifier, a silicon
377 diode with a C6 amplifier for a trigger and a ^{90}Sr source on top. A particle emitted by
378 the source traversed the sensor bulk and hit the silicon diode, triggering the analogue
379 signal readout. The source was left on the top for the course of the experiment. The
380 measurements, however, took place at discrete times. For every data point, approx-
381 imately 10^4 triggers were recorded. The offline analysis of the recorded signal pulse
382 amplitudes yielded a landau distribution for every data point. The resulting graph of
383 charge collection over time showed that the charge collection efficiency improves over
384 time. This is especially evident in the case of the two irradiated samples. S79 achieves
385 close to full efficiency whereas S52 reaches about 75 %. Both increases are significant.
386 After some time the signal stabilises. As expected, the signal of the non-irradiated
387 S37 did not change with time – this pure sCVD diamond sample had the maximum
388 collection efficiency from the start.

389 It should be noted that the ~ 2.28 MeV electrons emitted by this source are not
390 MIPs, because they sit far to the left on the Bethe-Bloch function and therefore
391 deposit more charge in the bulk than the regular MIPs. Nevertheless, for the purpose
392 of these measurements this energy was adequate since only the relative change in
393 charge collection was of our interest.

394 To sum up, diamond is an adequate material for use in β radiation detection.
395 Even if damaged by radiation, it reaches equilibrium in the order of an hour and
396 exhibits stable charge collection from then on. The efficiency decreases with received
397 radiation dose, but the decrease can be accounted for if the damage factor and the rate
398 energy of the particles are known. γ radiation has a similar impact on the diamond
399 as the β . The impinging photons, if they interact with the diamond, prime the bulk,
400 causing the increase in charge collection efficiency. The difference, however, is in the
401 interaction probability (cross section), which is several orders of magnitude lower for
402 gammas.

403 **α measurements**

404 This part discusses the stability of irradiated diamond sensors during α measure-
405 ments. It is justified to assume that they will behave differently than when subject
406 to β radiation. This is due to the point-like charge carrier creation when an α par-
407 ticle impinges the bulk. The energy is approximately 20 times higher than the most
408 probable value of a MIP; deposited in a small volume, it will behave differently to the
409 track-like energy deposition of MIPs. In addition, carriers of only one polarity drift
410 through the sensor while the others almost instantly recombine with the adjacent
411 electrode. Taking into account that the diamond bulk has been damaged by irradia-
412 tion, these two phenomena might have an effect on the operation of the detector on
413 a macro scale.

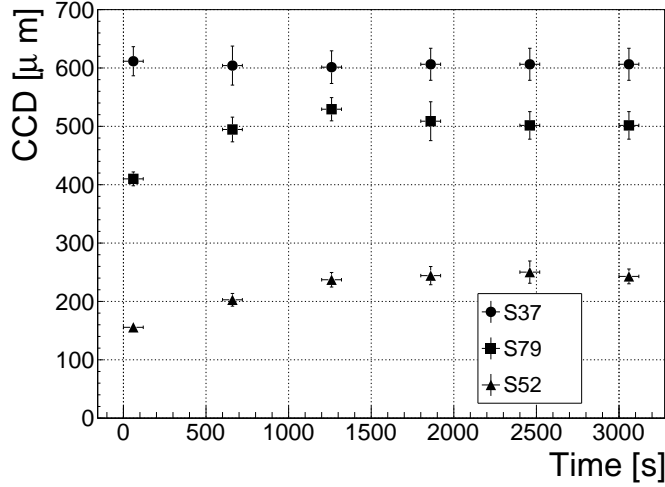


Figure 1.8: Increase of charge collection over time due to priming with the ^{90}Sr radioactive source

The measurement setup consisted of a PCB carrier for a diamond with a fitted ^{241}Am source and a vacuum chamber. The carrier was placed into the chamber, which was evacuated. It acted as shielding for external noise pickup and ensured that the α particles didn't lose energy traveling through air. An SMA feedthrough ensured the electrical connection to the outside. The samples were measured before and after priming, at both polarities, to compare the behaviour of both electrons and holes as charge carriers. The scope of the measurements was to observe the eventual changes in charge collection efficiency and/or in the pulse shapes.

The first test was carried out using the Cx spectroscopic amplifier. The bias voltage of the samples was set to +500 V and the signals from the diamond were measured for \sim 15 minutes. Figure 1.9 shows the results of these measurements. The collected charge for the non-irradiated sample was stable with time. It was expected that the irradiated samples will have a lower charge collection efficiency than their non-irradiated counterpart. However, their initial efficiency suddenly dropped after a certain period of time. Priming did improve their efficiency, but it only deferred its eventual drop. In addition, the spread of measured energies increased significantly. Also, the particle counting rate decreased with the decreased efficiency.

The next step was to observe the behaviour of the current pulse shapes with time using a C2 current amplifier. The shape of the pulse holds more information about the micro-processes in the sensor than solely the value of the integrated charge. This time only the primed sensors were tested. Both hole and electron collection were observed to determine whether they behave differently or not. The samples were measured long enough for the pulse shapes to start changing. The data in figures 1.10 show that the pulses start changing in a chaotic way – suddenly there are several different shapes, some still the same as at the beginning while the others with almost zero amplitude. These data are difficult to interpret. Nevertheless, the idea is that some charges get

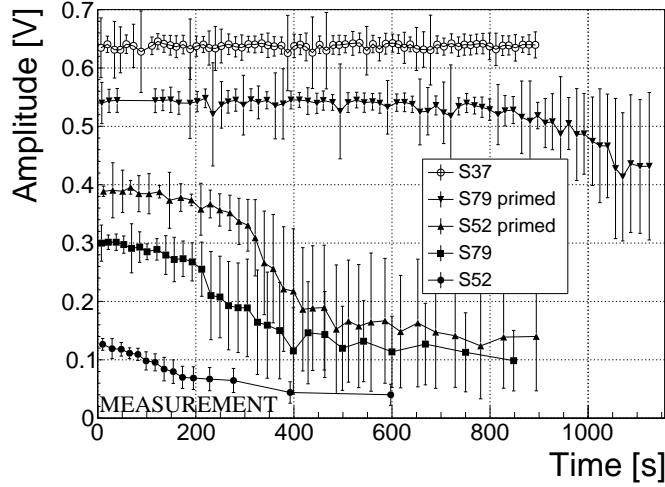


Figure 1.9: Comparison of collected charge with time for non-irradiated and irradiated diamond samples.

440 trapped in the charge traps in the bulk for a long time, building up regions of space
 441 charge. Since only one charge flavour is drifting through the bulk whereas the other
 442 is quickly recombined, this already determines the imbalance in spatial distribution
 443 of trapped charges. The built up space charge affects the electric field, making it
 444 non-uniform. The non-uniform field in turn affects the drifting carriers, slowing them
 445 down or speeding them up, depending on the field gradient. Since the movement of
 446 the carriers is the electric current, the field gradient can be observed in the signal.
 447 Unfortunately the effects are very convoluted, probably due to the impinging point
 448 of the α particle.

449 Finally, an effort has put into finding a way for the pulse shapes to return to
 450 their initial state. Five methods were tested: (1) Removing the source and leaving
 451 the bias voltage on, (2) Removing the source and switching the bias voltage off, (3)
 452 Priming with γ without bias voltage, (4) Priming with β with bias voltage on and
 453 (5) priming with β without bias voltage. The diamond sample S79 was first primed
 454 using a ^{90}Sr source for about one hour. Then the bias voltage was switched on and an
 455 ^{241}Am source was put on top. The pulses produced by the impinging α particles had
 456 a proper rectangular pulse at the beginning, but then started changing in an erratic
 457 way. After approximately 30 minutes, one of the methods was tested. Then the bias
 458 voltage was switched off and the sample was primed again to reset its state before
 459 starting with the next run.

460 At the beginning of every run, 60 reference pulses of the initial pulse were taken
 461 and plotted overlapped into a 2D histogram. An average pulse was extracted from this
 462 2D distribution. Then a correlation between the reference pulses and the averaged
 463 pulse σ_{ref} was calculated. When a "healing" procedure was started, a set of 60 pulses
 464 was taken at irregular points of time to observe the change in the pulse shape. At
 465 every data point the correlation with the initial averaged pulse σ was calculated. From

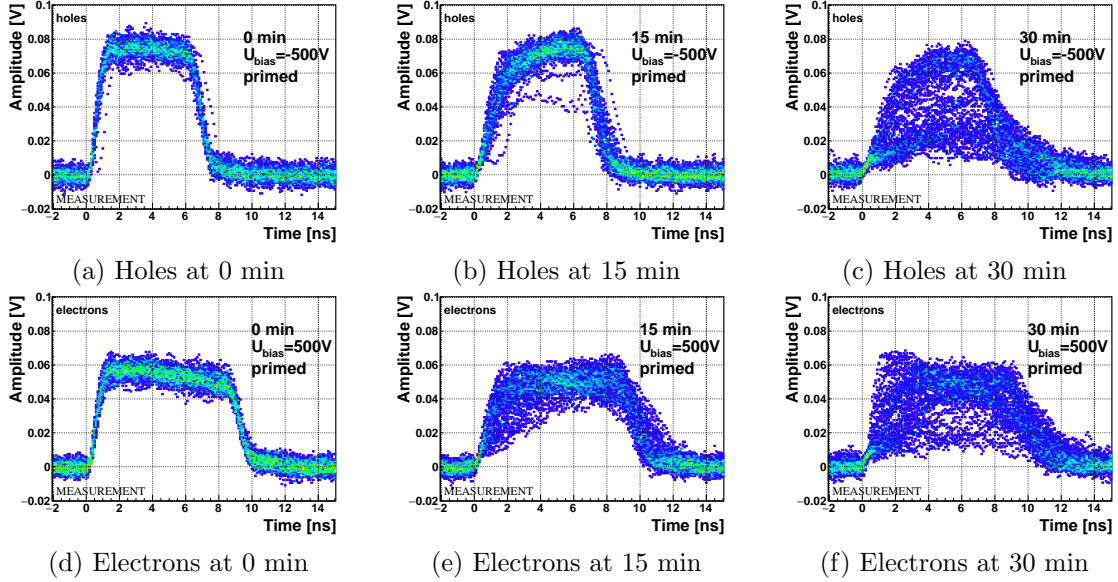


Figure 1.10: This plot shows the signal deterioration of the irradiated and primed S79 with time for both polarities. Every plot contains 60 superimposed pulses.

466 the initial correlation σ_{ref} and discrete correlation values σ in time, the correlation
 467 form $Corr_{form}$ was calculated and plotted against time on the plot in figure 1.11.

$$Corr_{form}(t) = \frac{\sigma_{ref}}{\sigma} = \frac{\sum_x \sum_y w_{ref} \cdot (y_{avg} - y_{ref})^2}{\sum_x \sum_y w \cdot (y_{avg} - y)^2} \quad (1.5)$$

468 It turns out that the methods (3) and (5) improve the form, method (2) helps slowly,
 469 (1) does not show any change with time and (4) at first improves, but then significantly
 470 degrades the shape. The effect observed in method (4) has already been described
 471 in [?]. The "healing" process therefore depends on the rate of radiation, the bias
 472 voltage and the time of exposure. The ionising radiation creates free charges, which
 473 quickly recombine close to the place of generation. It is likely that they also release
 474 the charges trapped during the measurement, reducing the overall effect of the space
 475 charge. The traps get filled with both flavours of carriers, thus they are neutralised.
 476 The pulse shape gradually returns to its initial state.

477

Procedure	Source	Bias voltage	Effectiveness
1	/	ON	no
2	/	/	slow
3	^{60}Co	/	YES
4	^{90}Sr	ON	no
5	^{90}Sr	/	YES

478

Table 1.2: Effectiveness of healing procedures

479

TO-DO conclusions: limitations

480

To sum up, the shape of the pulses caused by α radiation changes with time for
 481 irradiated samples. The form of the pulses gets distorted and becomes erratic. Charge

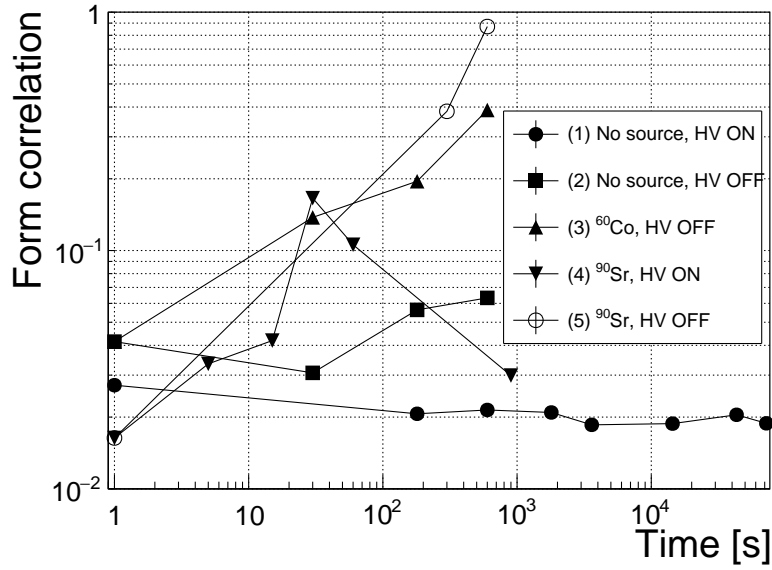


Figure 1.11: Five procedures of the "healing" process for an irradiated diamond that was exposed to α radiation at bias voltage switched on for at least 30 minutes.

⁴⁸² collection decreases and its spread increases. This happens even faster for non-primed
⁴⁸³ diamonds. To "heal" the diamond – to bring the pulse shapes back to their initial
⁴⁸⁴ form – the sample must be primed using a β or a γ source for several minutes at the
⁴⁸⁵ bias voltage set to 0 V. Switching to the inverse polarity for a few seconds helps a
⁴⁸⁶ bit, but in a long run distorts the signal, which cannot get back to its initial form.

487 1.4 Temperature limitations

488 A test was carried out to evaluate the effect of temperature changes on the output
 489 signal of the diamond sensors. A cryostat filled with liquid helium was used to
 490 cool down the sensor during the measurement process. Current signal response to
 491 α -particles was measured at 18 temperature points between 4 K and 295 K (room
 492 temperature - RT). At every temperature point, a set of 300 pulses was read out at
 493 various bias voltages. Resulting data showed that the charge collection is stable down
 494 to 150 K, where it starts decreasing and stabilises again at about one third of the
 495 initial value at 75 K. This behaviour was first measured and discussed by H. Jansen
 496 in [?].

497 The band gap energy in diamond equals to $E_g = 5.5$ eV while the average energy
 498 to produce an electron-hole pair is $E_{e-h} = 13.25$ eV. This means there is excessive en-
 499 ergy deposited in the diamond bulk. The impinging α -particle stops within $\sim 10 \mu\text{m}$
 500 of the bulk, transferring all its energy to the lattice. A part of this energy, approx-
 501 imately 40 %, directly ionises the carbon atoms, creating free electron-hole pairs.
 502 The remaining energy, however, is converted into lattice vibrations (phonons [?]).
 503 This effectively means that the lattice within the ionisation volume (approximately
 504 $\sim 10 \mu\text{m} \times \sim 2 \text{ nm}$ in size) is briefly heated up. The hot plasma then cools down to the
 505 temperature of the surrounding material by heat dissipation, (i.e. phonon transport).

506 The positively charged hole and negatively charged electron in the hole attract
 507 each other via the Coulomb force and may undergo a bonding process during which a
 508 phonon is emitted. That phonon is referred to as *exciton* [?]. The electron is pushed
 509 to a so-called exciton energy band, which is 80 mV under the conduction band. At
 510 higher temperatures, the lattice provides enough energy to excite the electron from
 511 the exciton state back to the valence band (so-called exciton recombination). At lower
 512 temperatures, however, the exciton lifetime increases, which means that it will take a
 513 longer time for the electrons to get re-excited to the valence band. The re-excitation
 514 lifetime at room temperature is ~ 30 ps, increasing to $\sim 150 \mu\text{s}$ at 50 K.

515 1.4.1 Temperature-variant α -TCT before irradiation

516 Three sCVD diamond samples were tested at the range of temperatures using the
 517 α -TCT technique. At each temperature point, the bias voltage was set to several
 518 positive and negative values. A set of 300 pulses was recorded at every data point
 519 and averaged offline. The resulting averaged pulses of sample S37 at the 260 K
 520 temperature point and a bias voltage of ± 400 V, ± 500 V and ± 700 V are shown in
 521 figure 1.12. The pulses induced by holes as charge carriers are shorter than those
 522 induced by electrons, confirming that holes indeed travel faster in diamond. The area
 523 of the pulse, however, is the same for both polarities, which corresponds to the fact
 524 that the same amount of charges is drifting in both cases.

525 Figure set 1.13 shows pulses at bias voltage set to ± 500 V across the range of
 526 temperatures between 4 K and 295 K – room temperature (RT). Several conclusions
 527 can be drawn by observing their shape. First, the pulse shapes change with decreasing

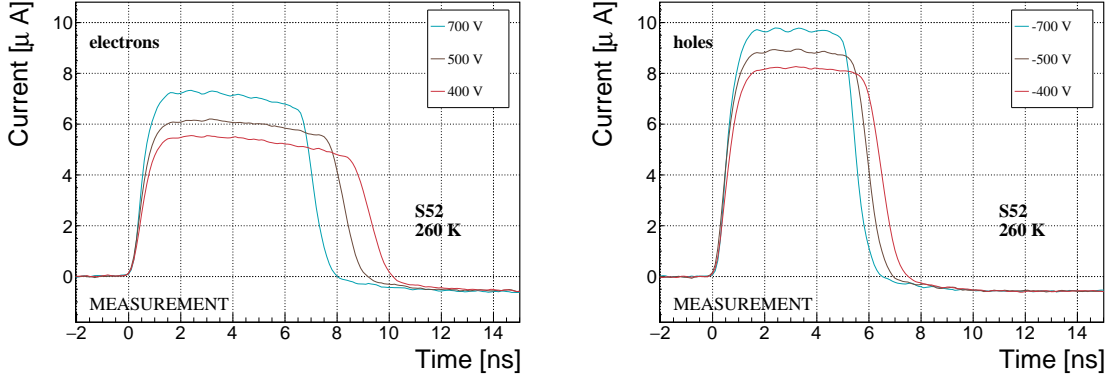


Figure 1.12: Varied bias voltage at a fixed temperature

temperature. The pulse time gets shorter, hinting at the faster carrier drift velocity v_{drift} . Second, between 150 K and 75 K there is a significant change in shape - the time constant of the rising edge increases significantly and the pulse area decreases. From 75 K down to 4 K there is no significant observable change. Last, the top of the pulse at the S52 is not flat, which means that a portion of the drifting charge is lost along its way. This could be due to impurities in the diamond bulk, which act as charge traps, or due to the space charge built up in the bulk. A linear pulse top hints on the latter. All in all, the pulse shape changes significantly with temperature, which is predicted by Jansen's model.

1.4.2 Temperature-variant α -TCT after irradiation

The irradiated S79 and S52 were re-tested in the cryostat. The aim was to see how their pulse shapes change with decreasing temperature, in particular the decaying top of the pulses (see figure 1.14). The decay time gives information on trapping of charge carriers while travelling through the diamond bulk. A variation of the decay time constant as a function of temperature might help to reveal the type and depth of the charge traps. To observe these effects (or lack thereof), a number of requirements had to be met. First, the diamond samples were intentionally not primed prior to the experiment because priming would improve the pulse shapes and the decaying tops. Second, keeping in mind that the pulse shape of irradiated diamonds changes with time, the length of the measurement of an individual data point had to be adequately short. Last, the sequence of the bias voltage settings was important, the reason for which is explained below.

Unfortunately it was not possible to avoid temporal pulse changes. For instance, one measurement point took approximately one minute. After the measurement, the bias voltage polarity was swapped for a few seconds to bring the diamond back into its initial state. But a few seconds with respect to a minute was not enough. Therefore, when the bias voltage was set to the next value, there was still some residual effect of the previous measurement. Similar to the effects of polarisation, this effect was

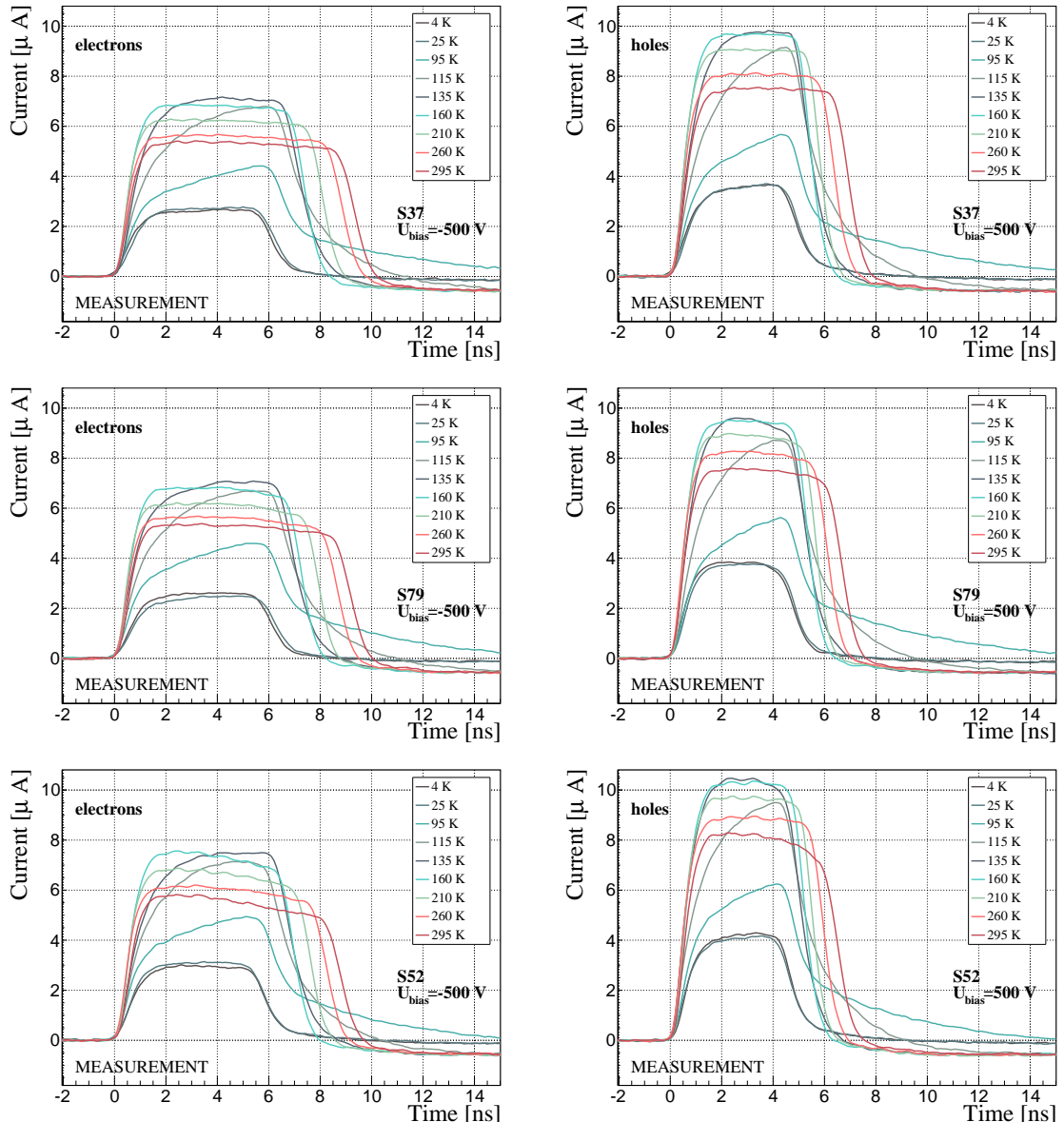


Figure 1.13: Several data points between 4 K and 295 K at a bias voltage of $\pm 500 \text{ V}$

also decreasing the pulse height. This can be observed in figure 1.14, which shows the resulting pulses of S52 for bias voltages of ± 200 V, ± 300 V, ± 400 V and ± 500 V at 230 K and 260 K. In this case the measurements sequence was: 230K (200 V, 300 V, 400 V, 500 V, -500 V, -400 V, -300 V), 260 K (-200 V, -300 V, -400 V, -500 V, 500 V, 400 V, 300 V). The changes in pulse shapes for holes at 230 K and 260 K cannot be attributed to the temperature change. Instead, the explanation could lie in diamond "*polarisation*". This means that, when exposed to an electric field with α measurements ongoing, the diamond builds up the internal electric field of inverse polarity, which effectively reduces the overall electric field. This internal field does not dissipate when the external bias voltage is switched off. It can be said that the diamond is "*polarised*". When switching the polarity of the external bias voltage, the internal and external electric field point in the same direction at the beginning, increasing the overall electric field and with it the pulse height. In figure 1.14, this happens when switching from 500 V to -500 V at 120 K. The built up polarisation contributes to the pulse having a sharp rising edge and a high amplitude. This effect decays during the next two voltage points. There would be a handful of ways to avoid this polarisation effect in the data: 1) after every data point invert the bias voltage and leave it to return to a neutral state for the same amount of time, 2) make a hysteresis of data points, going from minimum negative to maximum positive bias several times, 3) reduce the measurement time at every bias voltage setting. Unfortunately, possibility 1 and 2 are very time consuming and would increase the overall experiment time to over one day. The third option would worsen the resulting averaged pulses. In the end an alternative option was chosen: alternating the starting bias voltage and the sequence at every temperature point. With this option, the highest possible systematic error in analysing the pulse shapes could be attained.

Figure 1.15 shows the irradiated S52 and S79 as well as the non-irradiated S37 for comparison, all at a bias voltage of ± 500 V and at several temperature points between 4 K and RT. It is evident that the irradiation affected the shape of the pulses across all temperatures.

A decaying exponential function was fitted to the decaying top at pulses at bias voltages of ± 400 V and ± 500 V across all temperatures excluding the transitional range between 75 K and 150 K. There was a spread of fitted values at individual temperature points, stemming from the fact that the pulses changed with time due to "*polarisation*". This counts as a systematic error. Therefore all four fitted values were averaged into one value representing the measurement at that temperature point. Figure 1.16a shows the fitted decay time constants for the five samples between 4 K and 295 K. In principle, the time constants should be infinite for a perfect and non-irradiated sample. Here a slightly decreasing top due to space charge was already successfully fitted with an exponential function, resulting in a time constant of the order of 200 s^{-1} . This is also why the spread is enormous. For the irradiated samples, the fit becomes increasingly more meaningful. As seen in the plot, the fitted values of the irradiated samples are fairly stable across all temperatures. There is a slight increase in the decay time constant of the S52 from $(6 \pm 0.5) \text{ s}^{-1}$ above 150 K to

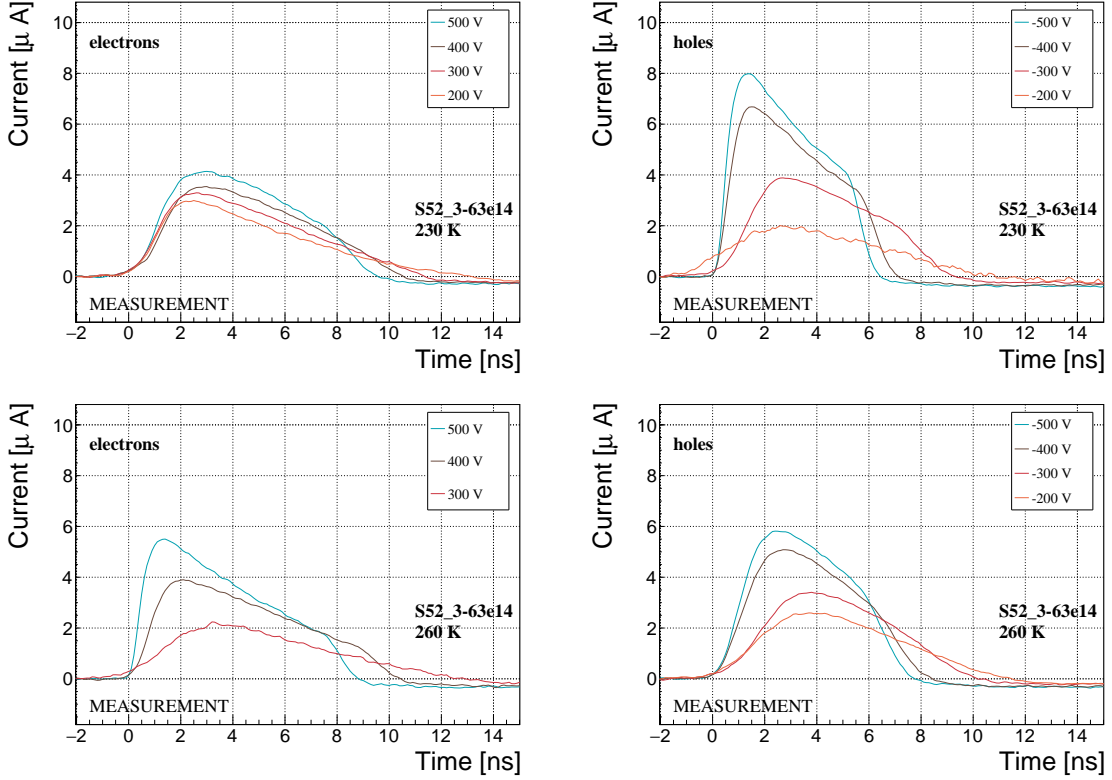


Figure 1.14: Varied bias voltage at a fixed temperature for an irradiated sample

(8.5 ± 0.9) s^{-1} below 75 K. On the other hand, this step is not observable in the S79 data. With only one sample exhibiting this behaviour, the effect is not significant enough. Judging by the data acquired, the samples would need to be irradiated to doses above $1 \times 10^{14} \pi \text{ cm}^{-2}$ to quantify this effect in detail. All things considered, this effect will not be regarded as significant for the scope of this thesis. Building on this assumption, the conclusion is that the signal decay time constant for irradiated sCVD diamond is constant across the temperature range between 4 K and 195 K, excluding the transitional range between 75 K and 150 K.

Taking into account the conclusions above, all the values can be averaged into one decay constant. Figure 1.16b shows these values for all samples plotted against received π radiation dose. To estimate the carrier lifetime with respect to the radiation dose received, a similar model was used than that in section 1.5. This model states that the inverse of the carrier lifetime is linearly decreasing with increasing radiation dose:

$$\frac{1}{\tau} = \frac{1}{\tau_0} + k_\tau \cdot \Phi \quad (1.6)$$

$$\tau = \frac{\tau_0}{k_\tau \tau_0 \Phi + 1} \quad (1.7)$$

where τ_0 is the lifetime for a non-irradiated sample (real lifetime, therefore of the order of 400 s^{-1}), τ is the lifetime of an irradiated sample, Φ is the received radiation

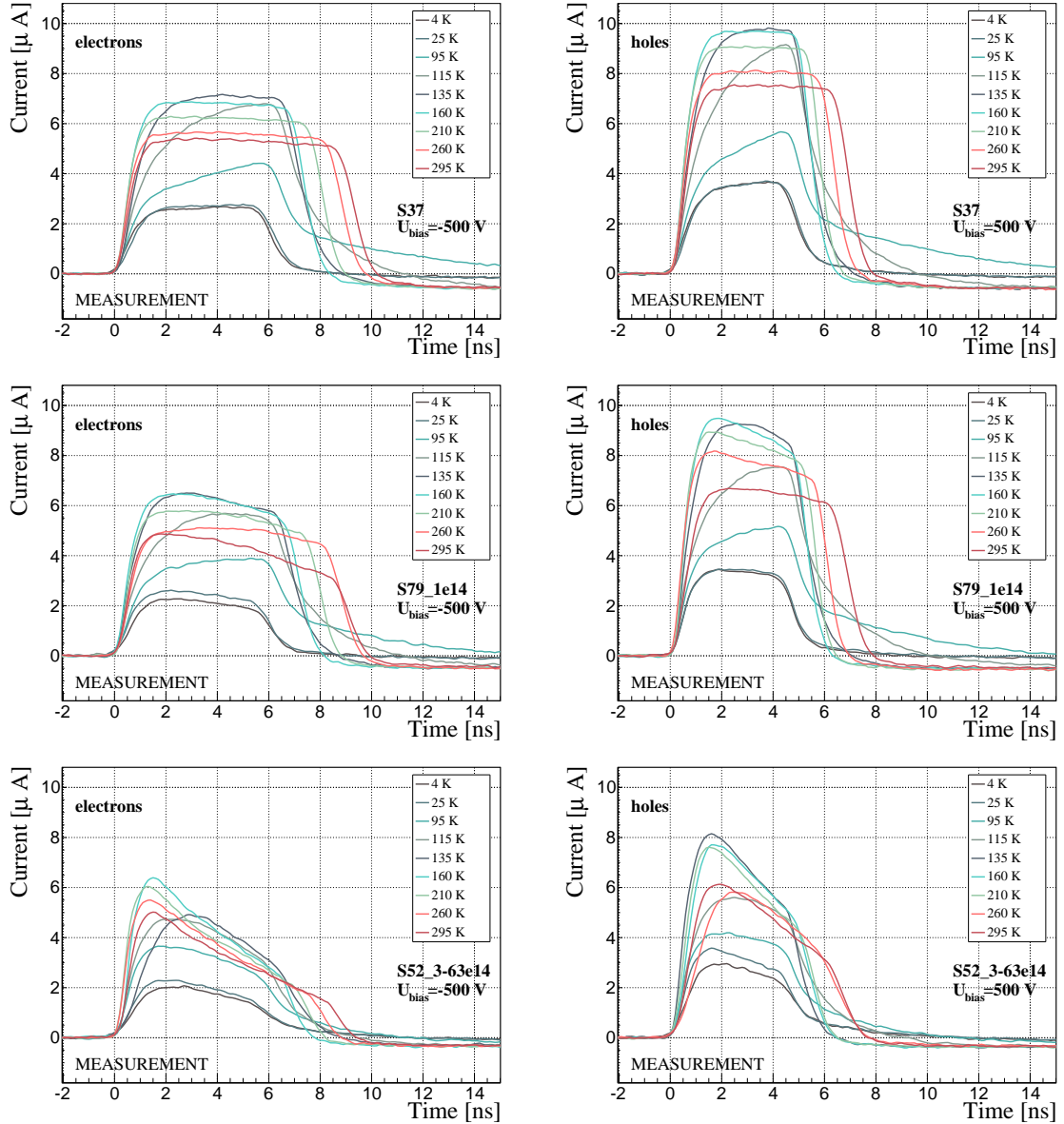
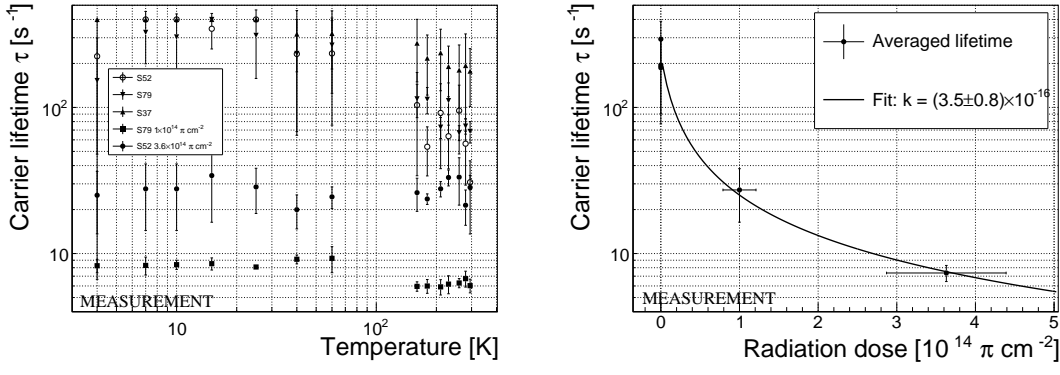


Figure 1.15: After irradiation: several data points between 4 K and 295 K at a bias voltage of ± 500 V

dose and k_τ the lifetime degradation factor. For these data the fitted factor was equal to $k_{tau} = (3.6 \pm 0.8) \times 10^{-16} \text{ s cm}^2 \pi_{300 \text{ MeV}}^{-1}$. Using this factor, the steepness of the decay in the pulse shape with respect to radiation dose can be estimated. This can help when designing a system where current pulse shape is an important factor.

620 1.5 Conclusion

621 This chapter gave an overview of the capabilities and limitations of diamond as a
 622 particle detector. Three effects on diamond were studied – noise, radiation and tem-



(a) Carrier lifetime as a function of temperature

(b) Carrier lifetime averaged over all temperatures as a function of π irradiation dose

Figure 1.16: Charge carrier lifetime decreases with irradiation, but is stable across the range of temperatures between 4 K – 75 K and 150 K – 295 K.

623 perature, the focus being on the latter two.

624 Two sCVD diamond detectors were irradiated with 300 MeV pions. They were
 625 tested alongside a non-irradiated sample to observe the changes in the ability to de-
 626 tect α , β and γ radiation. Their charge collection efficiency was measured in a test
 627 beam facility using . The results were compared to the results from the RD42 collab-
 628 oration and a DPA model provided by Karlsruhe Institute of Technology, Germany.
 629 A radiation damage factor $k = (3.0 \pm 1.0) \times 10^{-18} \mu\text{m}^{-1} \text{cm}^{-2}$ was obtained. The data
 630 point did not fully overlap with the data provided by RD42 nor the model. However,
 631 the irradiation process and the low number of tested samples hold a relatively high
 632 statistical uncertainty. These results will also be fed into the existing pool of data in
 633 the RD42 collaboration, increasing the otherwise rather low number of measurement
 634 points of irradiated diamond samples.

635 The next step was to test the long-term capabilities for α detection. The shape
 636 of the ionisation profile was investigated to determine the behaviour of the charge
 637 carriers in the irradiated diamond. An exponential decay was observed in the pulse,
 638 proving that there are charge traps in the bulk that were created during irradiation.
 639 Then a long-term stability test was carried out. The results show that the irradiated
 640 diamond detectors do not provide a stable and reliable long-term measurement of
 641 α particles. Presumably this is due to a space-charge build-up in the bulk, which
 642 changes the electric field, affecting the charge carriers. A procedure to improve the
 643 pulse shape using β and γ radiation was proposed.

644 Finally, the diamond sensors were cooled down to temperatures between 4 K and
 645 295 K. Their response to α particles was observed. The results of the non-irradiated
 646 and irradiated samples were compared. The effect of reduction for the number of
 647 drifting charges due to exciton recombination was observed in both sets of data.
 648 The second set had a superimposed effect of charge trapping during the drift, which
 649 was represented by an exponential decay in the signal. The decay time constant

650 did not change with temperature. Therefore all temperature points for individual
651 samples were averaged and the decay time constants were plotted against the received
652 radiation dose. A damage factor equal to $k = (3.6 \pm 0.8) \times 10^{-16} \text{ s cm}^2 \pi_{300 \text{ MeV}}^{-1}$ for
653 non-primed diamonds was defined.